Synthesis of Thick Mesoporous γ-Alumina Films, Loading of Pt Nanoparticles, and Use of the Composite Film as a Reusable Catalyst

Anirban Dandapat, Debrina Jana, and Goutam De*

Sol–Gel Division, Central Glass and Ceramic Research Institute, Council of Scientific and Industrial Research, 196 Raja S. C. Mullick Road, Jadavpur, Kolkata 700032, India

ABSTRACT Nanocrystalline mesoporous γ-Al_2O_3 film of high thickness has been developed and characterized. The films were prepared on ordinary glass substrates by a single dip-coating method using boehmite (AlOOH) sols derived from aluminum tri-sec-butoxide in presence of cetyltrimethylammonium bromide (CTAB) as structure-directing agent. The dried films were heat-treated at 500 °C in air to remove the organics and strengthen the network. The GIXRD of the heat-treated (500 °C) film shows a broad peak in the low-angle region supporting the formation of worm-hole-like disordered mesostructures. The high-angle GIXRD, FTIR, and TEM of the films confirm the formation of γ-Al_2O_3. N_2 adsorption–desorption analyses showed that the heat-treated (500 °C) film has a BET surface area of 171 $m^2\ g^{-1}$ with a pore volume of 0.188 $cm^3\ g^{-1}$ and mean pore diameter 4.3 nm. Pt nanoparticles (NPs) (~2.7 mol % with respect to the equivalent $AlO_{1.5}$) were generated inside the mesopores of the heat-treated films simply by soaking H_2PtCl_6 solutions into it, and followed by thermal decomposition at 500 °C. The surface area and pore volume of the Pt-incorporated film have been reduced to 101 $m^2\ g^{-1}$ and 0.119 $cm^3\ g^{-1}$ respectively, confirming the inclusion of Pt NPs inside the pores. FESEM and TEM studies revealed uniform distribution of Pt NPs (2–8.5 nm; average diameter 4.9 nm) in the films. Catalytic properties of the Pt-incorporated films were investigated in two model (one inorganic and other organic) systems: reduction of hexacyanoferrate(III) ions by thiosulfate to ferrocyanide, and *p*-nitrophenol to *p*-aminophenol. In both the cases, the catalyst showed excellent activities, and the reduction reactions followed smoothly, showing isosbestic points in the UV-visible spectra. The catalyst films can be separated easily after the reactions and reused several times.

KEYWORDS: mesoporous γ-Al_2O_3 film • CTAB • Pt nanoparticles • catalysis • reductions of hexacyanoferrate(III) and *p*-nitrophenol

1. INTRODUCTION

Efforts are underway to find suitable catalysts that are active and stable, easy to handle and separate from the reaction mixture, and reusable for several cycles. In particular, for industrial applications, catalyst recovery and recycling are very important issues when costly metals are involved. Intensive work is ongoing to develop mesoporous transition metal oxides (as-such and doped) (1–4) to enhance the catalytic activities because of their high surface area and continuous 3D pore structure. However catalyst poisoning, separation of catalyst after the reaction, reusability of the catalysts, etc., are known problems. Mesoporous film hosts could be one of the suitable candidates to avoid these problems. Work related to the synthesis of metallic nanoparticles hosted in sol–gel-derived mesoporous SiO_2/TiO_2 films (5) and their catalytic and photocatalytic activities was investigated. However, use of SiO_2/TiO_2/ZrO_2 films as support is limited because films of suitable quality (accessible pores with optimum hardness) of the order of a few micrometers can not be obtained in a single dipping technique. Synthesis of relatively thick mesoporous silica films (~1 μm) is possible using the inorganic–organic sol–gel route and subsequent heat-treatment. However, silica film has a tendency toward densification (which causes pore shrinkage, pore closure, and formation of ink-bottle pores) even at 500 °C. In the case of TiO_2/ZrO_2, the situation is even critical and thickness of alkoxide derived TiO_2 or ZrO_2 film can not be increased beyond about 0.15 μm. Relatively thicker mesoporous TiO_2 films (6) can be synthesized, but they are usually soft in nature. Mesoporous Al_2O_3 films could be one of the alternative materials to use as a catalytic support. Synthesis of surfactant templated mesoporous alumina powders using different types of ionic and nonionic surfactants is of current interest (7–9). Studies related to the synthesis of mesoporous alumina films are, however, few (10, 11). Although the reported film materials possess ordered structures, they are relatively thin (0.1–0.3 μm) or prepared at high temperature (10, 11), and their use as catalysis supports has not yet been established. It is worth mentioning here that the essential parameters of the mesoporous film support materials should meet the following important criteria from the practical application point of view: (i) the thickness of the film should be in the range of a few micrometers so that a reasonable amount of active materials can be incorporated, (ii) pores should be well-accessible and free from microporosity, (iii) the film should be prepared within the temperature of 500 °C so that ordinary glass can be used as substrates (otherwise it will

* Corresponding author. Fax:91-33-24730957. E-mail: gde@cgcri.res.in.
Received for review December 16, 2008 and accepted March 4, 2009

DOI: 10.1021/am800241x
© 2009 American Chemical Society

be expensive), and (iv) the film should be chemically inactive in the concerning reaction medium.

In this work, we attempted to prepare relatively thick mesoporous γ-Al_2O_3 films on the order of a few micrometers by a single-dip-coating technique of ordinary glass substrates using boehmite sols and CTAB as a structure-directing agent. As γ-alumina has applications in catalysis and boehmite is the preferred precursor to form γ-alumina (12), we have used boehmite sols to prepare the films. Among the noble metals, Pt is attractive because of its superior catalytic activities (13), so as an example we incorporated Pt nanoparticles (NPs) inside the above mesoporous alumina films to use them as a catalytic materials. We showed here that this thin film catalyst is easy to prepare, very active, very easy to separate from the reaction mixture, easy to reactivate after washing with water, and reusable several times without any significant degradation.

2. EXPERIMENTAL SECTION

Aluminium tri-sec-butoxide $Al[OCH(CH_3)C_2H_5]_3$ (ASB), potassium ferricyanide $K_3[Fe(CN)_6]$, sodium thiosulphate $Na_2S_2O_3$, and *p*-nitrophenol were supplied by Merck, $NaBH_4$ was purchased from Sigma-Aldrich and chloroplatinic acid, $H_2PtCl_6 \cdot xH_2O$, hydrochloric acid (HCl), cetyltrimethylammonium bromide (CTAB), and 1-propanol were supplied by Ranbuxy fine chemicals and s.d. fine chem limited. Laboratory-prepared double distilled water was used.

Preparation of Mesoporous Alumina Film. Boehmite (AlOOH) sol was first prepared by hot hydrolysis (>80 °C) of ASB and subsequent peptization of boehmite precipitates using HCl (14). The molar ratios of water/ASB and HCl/ASB were 100 and 0.10, respectively. After peptization, the sol was stirred vigorously under refluxing condition for 5 h and then kept another 48 h under refluxing condition. The sol is then concentrated to about 8 equivalent wt % $AlO_{1.5}$ content by distilling off the secondary butanol and a part of water. The required amount of methanol was then added to the sol to maintain the $AlO_{1.5}$ content at 5.3 wt %. The calculated amount of CTAB (0.05 mol % with respect to equivalent amount of $AlO_{1.5}$ present in the sol) was dissolved in a water/1-propanol (3:7 wt/wt ratios) mixture and this solution was mixed with the boehmite sol (5.3 wt %) with stirring and used for coating preparation.

Prior to coating deposition, the glass slides were thoroughly cleaned following the method reported earlier (15). The coatings were prepared by single dipping technique using a Dip-master 200, (Chemat Corporation, USA) with a withdrawal velocity of 6 in min^{-1}. Coatings were first dried at 60 °C for 20 min followed by heat-treated at 300 and 500 °C (ramp of 2 °C min^{-1}) with a holding time of 60 min in each stages. The thickness of final heat-treated (500 °C) coatings was 2.3 ± 0.1 μm (measured with a profilometer) and checked by FESEM.

Pt-Loading. The final heat-treated (500 °C) alumina films deposited on ordinary glass slides were soaked in 0.05 M H_2PtCl_6 solution (in 1-propanol) for 2 min. The soaked films were dried at 60 °C for 20 min followed by being heat-treated at 300 and 500 °C in air with a holding time of 30 min in each stage in a cumulative manner.

Characterization of the Film. The thickness of the coatings was measured by a Surfcorder SE-2300 profilometer (Kosaka Laboratory Ltd., Japan). Infrared absorption spectra of the films deposited on both side polished silicon wafers (intrinsic) were recorded by FTIR spectrometer (Nicolet, 380) with 200 scans for each sample. The UV−Vis spectra of films deposited on glass substrates were obtained using a Cary 50 scan spectrophotometer. GIXRD and FESEM micrograph of the heat-treated films (500 °C) were recorded using Rigaku SmartLab (operating at 9 kW using the rotating anode and cross-beam optics to enhance the X-ray intensity) and ZEISS SUPRA 35VP field-emission scanning electron microscope respectively. Nitrogen adsorption-desorption isotherms were collected at −196 °C using Quantachrome Autosorb 1 (BET and BJH models, respectively, for surface area and porosity evaluation) on film samples scratched off of the substrate. Transmission electron microscopic (TEM) measurements were carried out with a JEOL 2010 operating at 200 kV and Tecnai G^2 30ST (FEI) operating at 300 kV transmission electron microscopes.

Estimation of Pt by ICP-ES. Quantitative estimation of Pt inside the films was performed using Perkin Elmer Optima 2100 DV inductively coupled plasma emission spectrometer (ICP-ES). For this purpose, the H_2PtCl_6 solution (0.05 M) soaked films (approximate dimensions 1.4 cm × 1.4 cm × thickness 2.3 μm × 2 surfaces) were first dried at room temperature and the film was then dipped in 10% HCl solution and kept under ultrasonication for 10 min to leach out the incorporated $PtCl_6^{2-}$ ions. The process was repeated for 4 times and the leached solutions were mixed together and analyzed (16). In the final 25 mL of solution (after volume adjustment), 10% HCl and 1% HNO_3 were maintained. The amount of Pt was estimated to be 7.88 mg/L (average of 3 sets of analysis). The amount of Pt was then reported as mol % with respect to the $AlO_{1.5}$ considering the density of the alumina film 2.1 g cm^{-3} (obtained by surface area−porosity measurements).

Catalytic Activities. For catalytic study, two pieces of these films (dimensions: 1.5 cm × 0.75 cm × 2.3 μm × 2 surfaces) were dipped in the mixtures of (i) $K_3[Fe(CN)_6]$ (1.25 mL; 1×10^{-3} M) and $Na_2S_2O_3$ (1.25 mL; 1×10^{-2} M) solution (13, 17) previously maintaining a temperature at 55 °C; and (ii) *p*-nitrophenol (0.15 mL; 1×10^{-3} M), water (2.7 mL), and $NaBH_4$ (0.15 mL; 0.1 M) solutions (18). The evolution of absorption spectra due to the reduction of $Fe(CN)_6^{3-}$ to $Fe(CN)_6^{4-}$ and *p*-nitrophenol to *p*-aminophenol have been recorded using a Agilent 8453 UV−visible spectrophotometer attached with a Peltier temperature controller (IACS, Kolkata) and Cary 50 scan spectrophotometer, respectively. Spectra were also recorded in the absence of catalysts.

3. RESULTS AND DISCUSSION

The heat-treated (500 °C) mesoporous γ-Al_2O_3 films deposited on glass substrate are transparent and crack-free. The final film thickness can be adjusted up to about 3 μm. The evolution of γ-Al_2O_3 films has been monitored by the grazing incidence X-ray diffraction (GIXRD) studies (Figure 1). The dried (60 °C) and heat-treated (300 and 500 °C) films (Figure 1a) show a broad peak in the low-angle region indicating formation of worm-hole-like disordered mesopores (7). In the case of dried film (60 °C), a relatively less broad peak centered at ~1.62 °2θ (d-spacing ≈ 5.4 nm) has been observed. Heat-treatment causes further peak-broadening and the peak has been shifted towards higher angle region at ~2.32° (d ≈ 3.8 nm) and ~2.36 °2θ (d ≈ 3.7 nm) in the cases of 300 and 500 °C treated samples, respectively (Figure 1a). This result suggests shrinkage of pores after the elimination of surfactants. The high-angle GIXRD patterns (Figure 1b) of the 60 and 300 °C treated films show peaks of boehmite phase (JCPDS card no. 17−0940), whereas the film heat-treated at 500 °C shows peaks corresponding to the γ-Al_2O_3 (JCPDS card 10−0425) phase. So, the film retains the boehmite structure after the elimination of surfactants at 300 °C and then transformed into the γ-Al_2O_3. The broad nature of high-angle peaks observed in all these cases

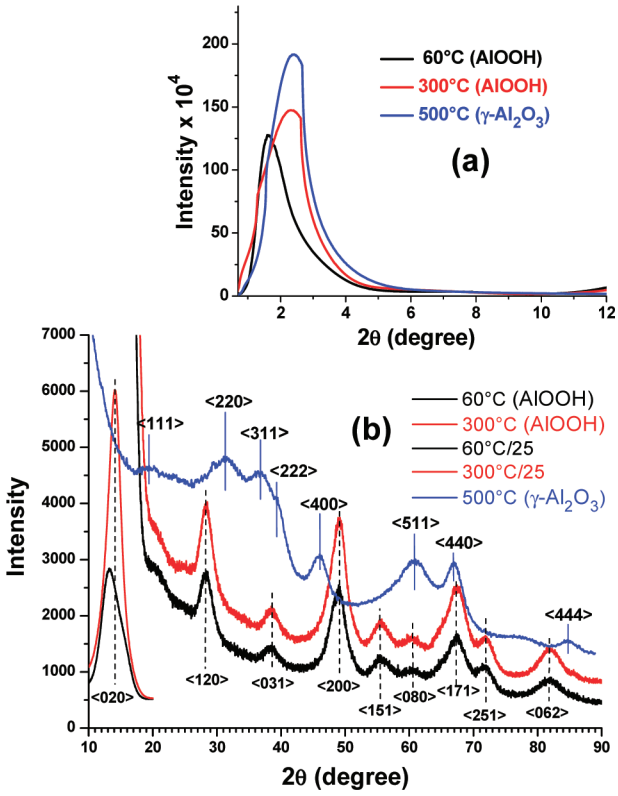

FIGURE 1. GIXRD pattern showing the formation of mesoporous γ-Al_2O_3 film after the thermal treatment of boehmite (AlOOH) films: (a) low-angle and (b) high-angle regions. The temperatures and corresponding crystalline phases are indicated in the body of the figure. The intensity of the AlOOH ⟨020⟩ peak in the cases of the 60 and 300 °C samples appears too strong. To show this peak, we have divided the intensity data (Y-axis) by a factor of 25 and shown them separately.

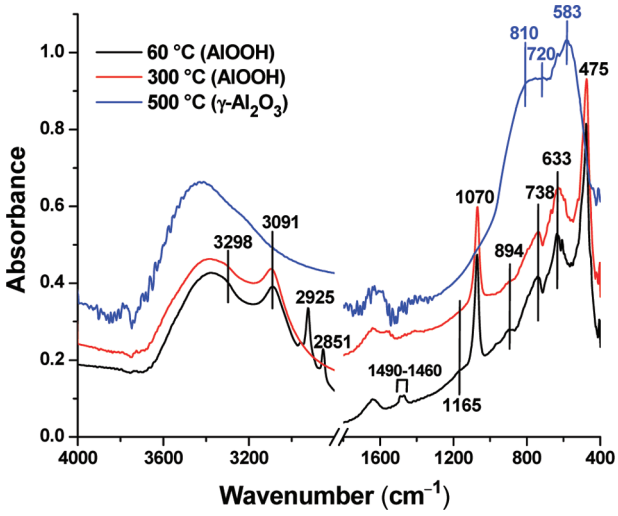

FIGURE 2. FTIR spectra showing the transformation of boehmite to γ-Al_2O_3 films after heat treatments. The film was deposited on a both sides of a polished intrinsic Si wafer.

suggests nanocrystalline structure. The FTIR spectra (Figure 2) of the dried (60 °C) film shows presence of peaks at 3298, 3091, 1165, 1070, 894, 738, 633, and 475 cm^{-1}, all attributed to the boehmite phases (14, 19), and at 2925, 2851, and 1490−1460 cm^{-1} region due to the organics. After heat-treatment at 300 °C, the organic peaks vanished (see the absence of $-CH_2$ stretching peaks at 2925 and 2851 cm^{-1}; Figure 2) but other peaks due to boehmite phase remains unaltered. Heat-treatment at 500 °C causes decomposition of boehmite and, as a consequence, the corresponding FTIR spectrum shows the disappearance of boehmite peaks at 3298, 3091, 1165, and 1070 cm^{-1} (19). At this stage, the spectrum shows broad peaks near 810, 720, and 583 cm^{-1}. Appearance of these peaks suggests the formation of γ-Al_2O_3 phase (19). It is evident that the boehmite film has been transformed to the γ-Al_2O_3 phase after heat-treatment at 500 °C in air, as confirmed by the GIXRD studies.

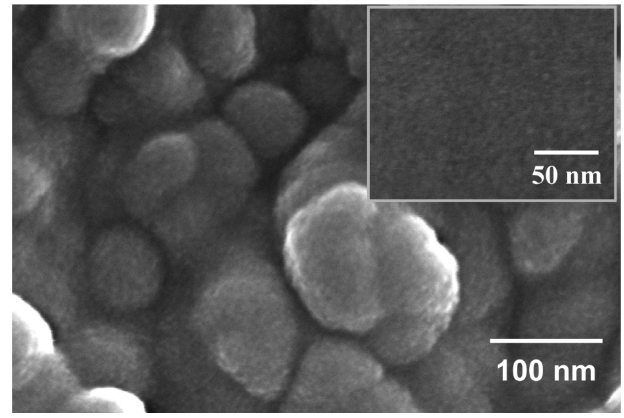

FIGURE 3. FESEM image showing the fracture surface of the mesoporous γ-Al_2O_3 film heat-treated at 500 °C. The inset shows the top surface of the film.

Figure 3 shows the field emission scanning electron microscopy (FESEM) image of the fractured and the top surfaces (inset) of the γ-Al_2O_3 film obtained after heat-treatment at 500 °C. FESEM image of the fractured surface shows that the film has a cauliflower-like internal structure composed of relatively large granular grains of about 50 nm in size and existence of fine pores in these granular grains, whereas the top surface (inset of Figure 3) shows only the fine pores. The TEM images of this film are shown in Figure 4. TEM (Figure 4a) shows an interconnected spongelike mesoporous structure of the film with pore sizes of about 4−5 nm. The corresponding selected area electron diffraction (SAED) pattern (Figure 4b) confirms the formation of γ-Al_2O_3 crystalline phase. The surface area and porosity of this mesoporous γ-Al_2O_3 films (before and after Pt incorporation) were evaluated using N_2 adsorption−desorption analyses at −196 °C. Panels a and b in Figure 5 show the plots of N_2 adsorption−desorption isotherms and pore size distributions, respectively. The pore size distribution (Figure 5b) of the γ-Al_2O_3 film falls well in the mesoporous region and is comparable with mesoporous alumina powders prepared using CTAB as a structure directing agent (7). The hysteresis loop in the desorption isotherm (Figure 5a) suggests the existence of some bottle-neck type pores. The undoped γ-Al_2O_3 film has a multipoint BET surface area of 171 $m^2\,g^{-1}$, with a mean pore diameter of 4.3 nm calculated from the adsorption bench of the isotherm (BJH method). The mean pore diameter appears slightly larger compared to the *d*-spacing value (~3.7 nm) obtained by the GIXRD. However, considering the broad nature of peaks, these values are comparable, and previously, larger differences of

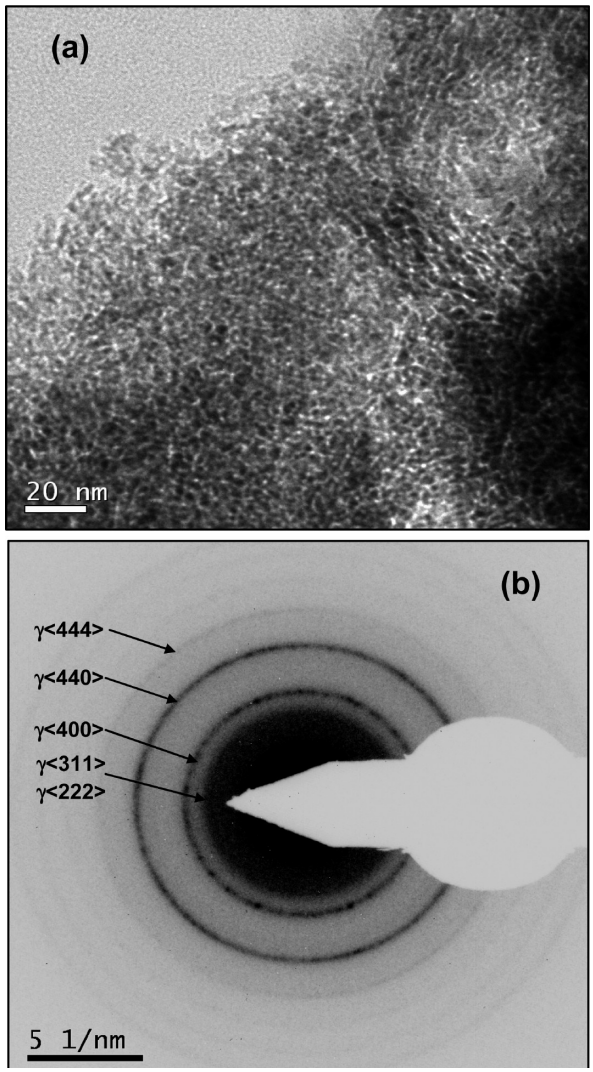

FIGURE 4. TEM image showing (a) the structure of mesoporous γ-Al_2O_3 film heat-treated at 500 °C, and (b) the SAED pattern obtained from (a).

such values in case of mesoporous alumina materials are reported (7b, 8b). The surface area (171 m^2 g^{-1}) of the γ-Al_2O_3 film is found to be little less than the corresponding bulk powders (7). However, considering the nanocrystalline nature, high skeleton density, and thin film structure, the surface area value is not low, and is comparable or higher than the nonsilicate mesoporous films (20). The volume percent porosity, pore volume, and density values of the films calculated from such BET analyses are found to be about 41 %, 0.188 cm^3 g^{-1}, and 2.1 g cm^{-3}, respectively. For Pt incorporation, the γ-Al_2O_3 films are soaked in H_2PtCl_6 solution and heat-treated at 500 °C to generate Pt NPs inside the mesopores. The N_2 adsorption–desorption analyses of this Pt-incorporated film (Figure 5a) shows surface area and pore volume values of 101 m^2 g^{-1} (59.1 % decrease compared to the undoped film) and 0.119 cm^3 g^{-1} (63.3 % decrease compared to the undoped film), respectively. The decrease of surface area and pore volumes after the incorporation of Pt NPs confirms that the Pt NPs are located inside the mesopores of γ-Al_2O_3 film. Further, a comparative analysis of the pore size distribution curves (Figure 5b) of

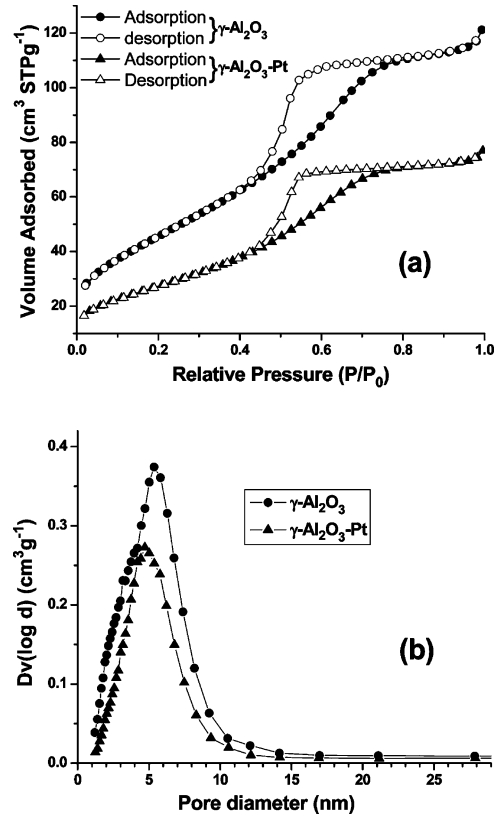

FIGURE 5. N_2 adsorption–desorption studies of the mesoporous γ-Al_2O_3 support film heat-treated at 500 °C and the corresponding Pt NPs incorporated (γ-Al_2O_3–Pt) films at −196 °C: (a) isotherms and (b) pore size distributions. The heat-treated films are scratched from the substrate using a steel knife and are used for this study.

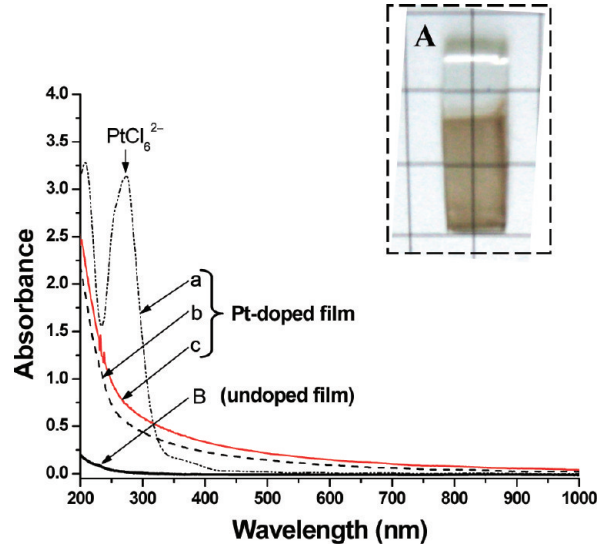

FIGURE 6. UV–visible spectral evolution of H_2PtCl_6 incorporated mesoporous γ-Al_2O_3 films heat-treated at different temperatures: (a) 60, (b) 300, and (c) 500 °C. The photo of the final heat-treated film (spectrum shown in red color), which has been used for catalytic studies is shown in the inset (marked by A). The spectrum of the undoped film heat-treated at 500 °C is also shown (marked by B).

γ-Al_2O_3 (undoped) and the corresponding Pt NPs incorporated films reveals a distinct shifting of pores towards the smaller dimensions, which also supports inclusion of Pt NPs inside the mesopores.

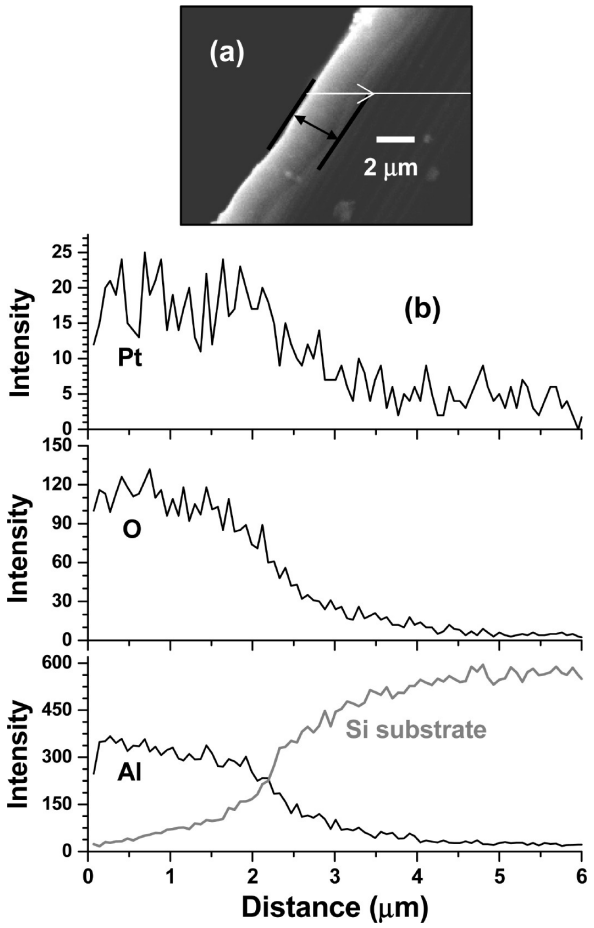

FIGURE 7. FESEM-EDS line scanning analysis along the thickness of the Pt-incorporated mesoporous γ-Al_2O_3 film (500 °C) used for catalytic studies: (a) cross-section image of the film; the black double-headed arrow shows the film thickness and the white line with arrow depicts the EDS scanning line; (b) intensity distributions of Pt, O, Al, and Si along the distance.

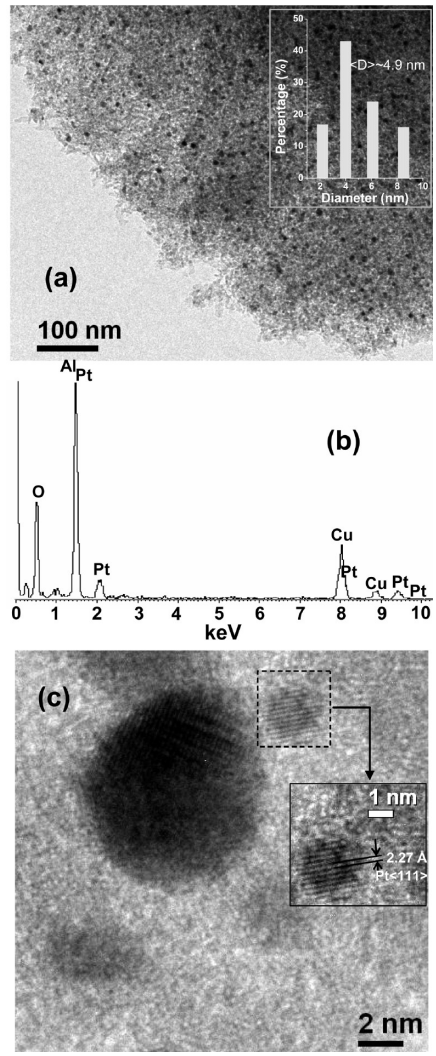

FIGURE 8. TEM studies of the Pt- incorporated mesoporous γ-Al_2O_3 film (500 °C) used for catalytic studies: (a) low-resolution image showing the structure of the mesoporous film and embedded Pt NPs (inset shows the size distributions of Pt NPs); (b) a representative EDS pattern showing the elements present in the film excepting Cu, which originated from the Cu grid used for TEM study; (c) high-resolution image showing fcc Pt NPs.

The H_2PtCl_6-solution-incorporated film, after being dried at 60 °C, shows a strong peak at ~271 nm due to $PtCl_6^{2-}$ ion (Figure 6) (21). Upon heat-treatment (300−500 °C) the $PtCl_6^{2-}$ ions are completely decomposed to Pt NPs, and as a result, the peak observed at 271 nm due to $PtCl_6^{2-}$ ions disappears, and the films show absorption with a gradual increase in intensity in the entire visible to UV regions, characteristics of Pt NPs (Figure 6; curves b and c) (21, 22). After heat-treatment at 500 °C, the film looks brown in color. A photo of this final heat-treated (500 °C) film deposited on glass substrate is shown in the inset of Figure 6. The equivalent Pt inside the films has been estimated using ICP-ES. The details are given in the Experimental Section (16). From such ICP-ES analysis the amount of loaded Pt in the film was found to be 2.7 ± 0.2 mol % (average of 3 analyses) with respect to the $AlO_{1.5}$. We performed FESEM-EDS line scanning analyses of the Pt-loaded film (Figure 7a) deposited on Si-wafer to reveal the concentration profile of Pt along the depth of the film. The EDS profile of Pt (Figure 7b) confirms uniform distribution of Pt along the film thickness (~2.3 μm). This result indicates that the film pores are well accessible, and for this reason, the Pt-solution reached uniformly inside the films. The profiles of oxygen, Al (from film), and Si (substrate) are also shown along the film thickness (Figure 7b). The transmission electron microscopy (TEM) studies of the Pt-loaded film are presented in Figure 8. As expected, the low-resolution (TEM) image of the Pt-doped, heat-treated (500 °C) film shows (Figure 8a) spongelike porous structure of the matrix films with highly dispersed Pt NPs of size ranges 2−8.5 nm (average size 4.9 nm). The size distributions estimated from such TEM image has been presented in the inset of Figure 8a. The corresponding TEM-EDS analysis (Figure 8b) shows presence of mainly Al, O, and Pt. The peaks of Cu appear from the Cu grid used for TEM study. The composition with respect to the atomic ratio of Al:Pt estimated from such TEM-EDS analysis is found to be 97.1:2.9 (average of three data), which is close to the ICP-ES analysis. The high-resolution TEM image showing both the small and relatively bigger Pt NPs is shown in Figure 8c. The adjacent lattice fringe spacing obtained from the high-resolution image of Pt NPs (Figure 8c) confirms its fcc structure. The selected area electron

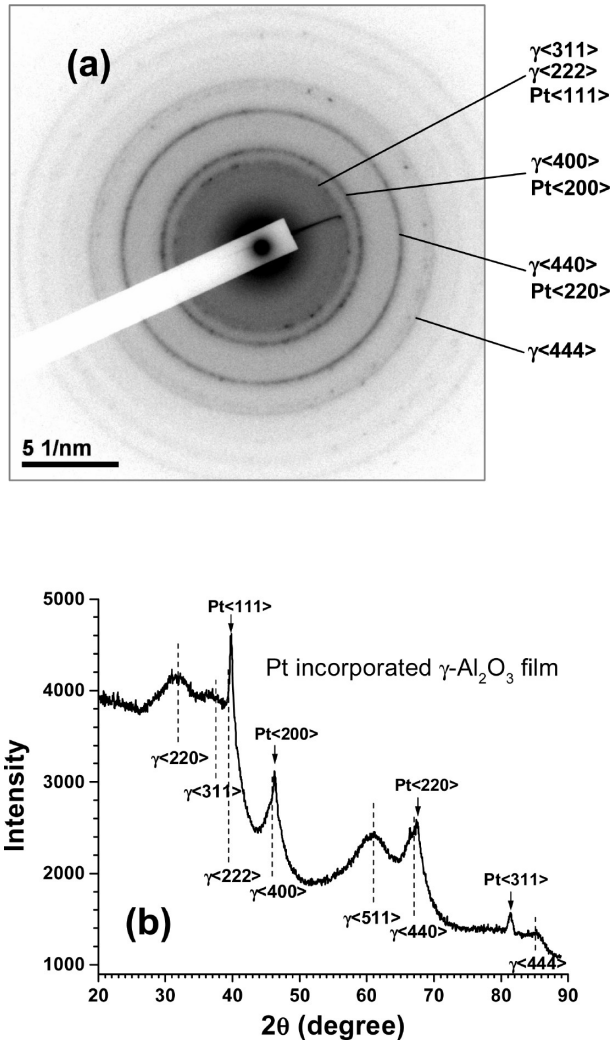

FIGURE 9. (a) SAED pattern obtained from the TEM image shown in Figure 8a; (b) GIXRD pattern of the Pt-incorporated mesoporous γ-Al_2O_3 film.

diffraction (SAED) pattern obtained from the low-resolution TEM (Figure 8a) is presented in Figure 9 along with the high-angle GIXRD pattern. The SAED pattern (Figure 9a) matches well with the γ-Al_2O_3 crystalline structure. It is however, difficult to identify the Pt lines from this SAED pattern because the broad nature of the γ-Al_2O_3 lines superimposes the Pt lines. The corresponding GIXRD pattern of the Pt-loaded film (Figure 9b), however, clearly resolved the fcc Pt and the γ-Al_2O_3 reflections.

The catalytic property of this Pt-loaded mesoporous γ-Al_2O_3 film (1.5 cm × 0.75 cm × 2.3 μm × 2 nos.) has been investigated in two different systems: (i) the typical redox reaction between $Fe(CN)_6^{3-}$ and $S_2O_3^{2-}$ at 55 °C and (ii) reduction of *p*-nitrophenol by $NaBH_4$ at 22 °C. For these studies, the optical spectra of the respective solutions in presence of such film catalysts were monitored with respect to time using UV−visible spectrometer and the results are presented in Figures 10 and 11, respectively. Figure 10a shows the successive UV−visible absorption spectra of the solutions recorded during the redox reaction between $Fe(CN)_6^{3-}$ and $S_2O_3^{2-}$. As shown in the figure, the depletion of $Fe(CN)_6^{3-}$ peaks have been observed as the reaction

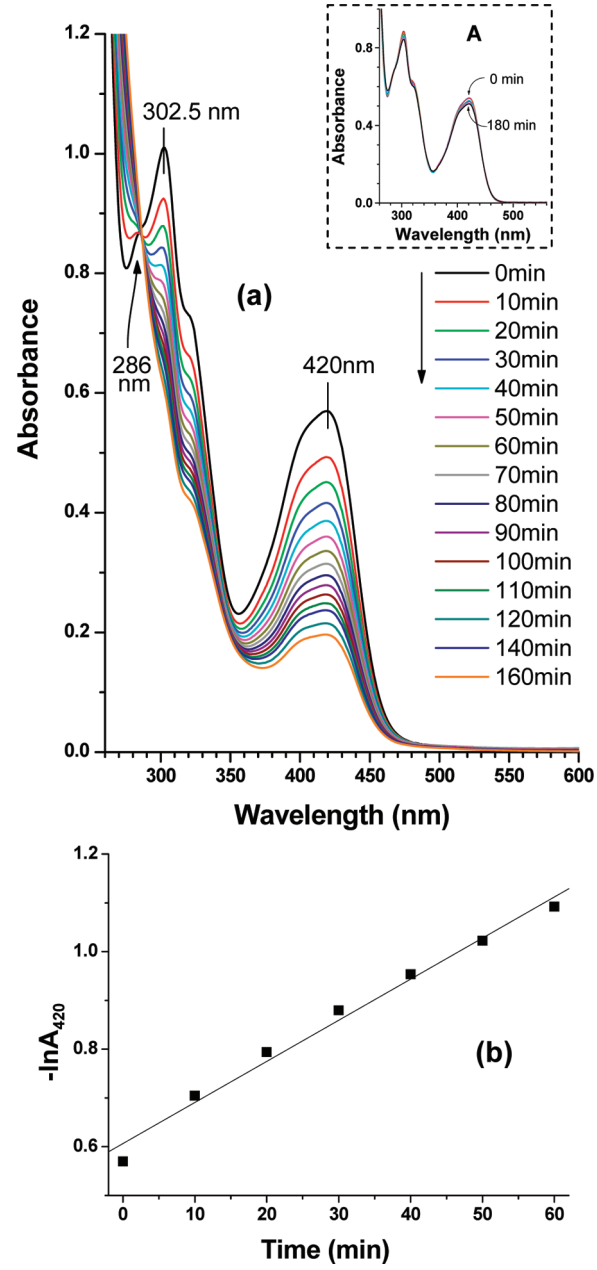

FIGURE 10. (a) Spectral change of $Fe(CN)_6^{3-}$ during the reaction between $Fe(CN)_6^{3-}$ and $S_2O_3^{2-}$ at 55 °C in the presence of Pt-incorporated mesoporous γ-Al_2O_3 film catalyst; inset shows the spectral change in presence of support alumina film (without Pt) or absence of catalyst film; (b) pseudo-first-order plot of −ln *A* (absorbance intensity at 420 nm) versus time for the above reaction in presence of film catalyst as shown in (a).

proceeds with time in the presence of Pt-loaded film. Similar tests in the presence of undoped film as well as absence of film were also studied and a very small change of absorption values (see inset of Figure 10a marked by A) were observed over a period of 180 min at 55 °C. It may be noted here that the reaction proceeds through a clear isosbestic point at 286 nm (Figure 10a), indicating that this redox reaction is proceeding smoothly without forming multiple products. The depletion of the 420 nm peak has been used to study the rate of such a catalyzed reaction. For this purpose, a plot of $-\ln A_{420}$ against time has been drawn and presented in Figure 10b. The rate constant (*k*) value for the above reaction

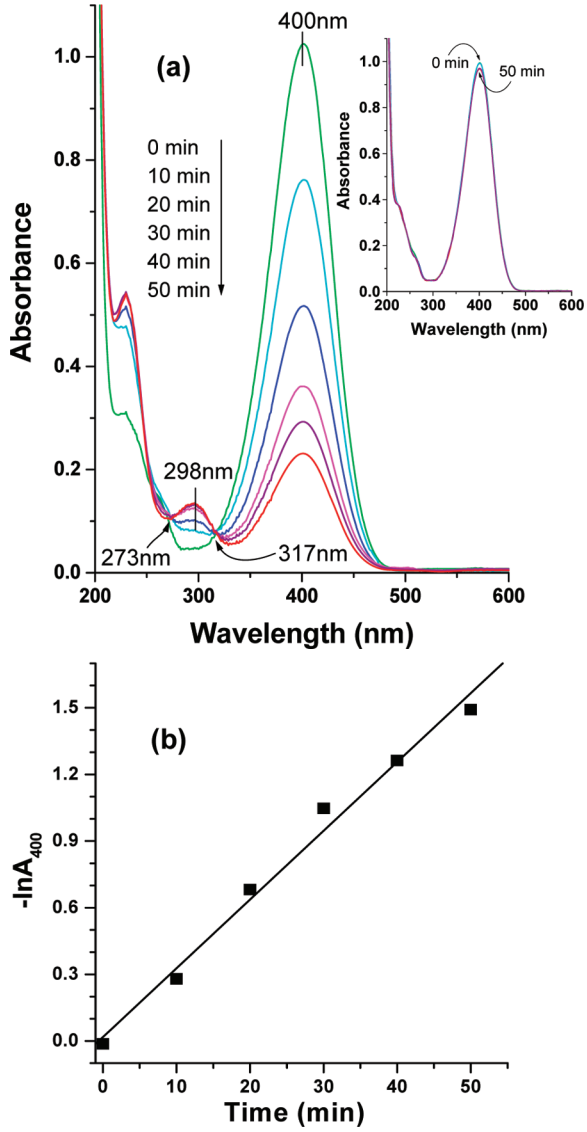

FIGURE 11. (a) Spectral change of *p*-nitrophenol during the reaction between *p*-nitrophenol and $NaBH_4$ at 22 °C in the presence of Pt-incorporated mesoporous γ-Al_2O_3 film catalyst; inset shows the spectral change in presence of support alumina film (without Pt) or absence of catalyst film; (b) pseudo-first-order plot of −ln A (absorbance intensity at 400 nm) versus time for the above reaction in the presence of film catalyst as shown in (a).

has been determined from the slope of the straight line and found to be 8.5×10^{-3} min^{-1}. This value is comparable with the reported *k* values using bare Pt NPs with comparable concentrations (13) where separation/regeneration of catalysts after the reaction was difficult.

In the case of reduction of *p*-nitrophenol, a decrease in the *p*-nitrophenol peak at 400 nm has been observed with respect to time with the concomitant appearance of a new peak at 298 nm because of the formation of *p*-aminophenol (Figure 11a). In this case, the reaction proceeds smoothly, showing two clear isosbestic points at 317 and 273 nm (Figure 11a) respectively. Similar reactions in the presence of undoped film as well as the absence of film show a very small change of absorption values of *p*-nitrophenol at 400 nm (see inset of Figure 11a). Figure 11b shows a plot of −ln A_{400} against time for this catalytic reaction, and the rate

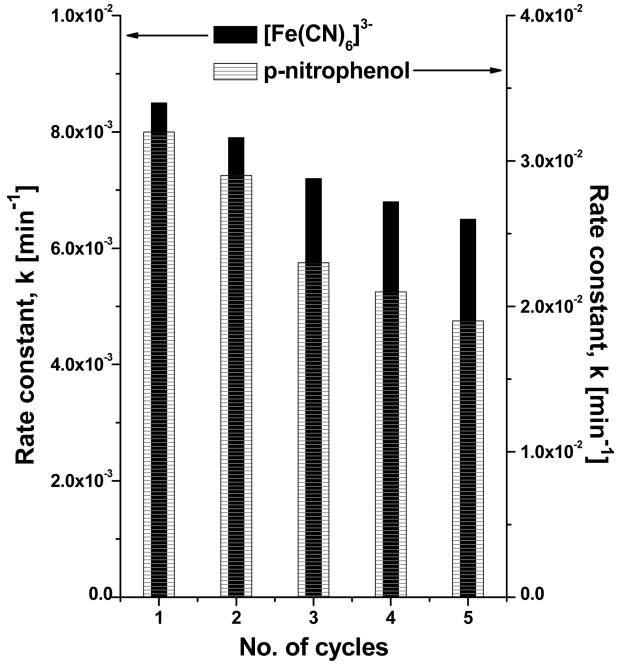

FIGURE 12. Rate constant values (*k*) of the catalytic reduction reactions of $Fe(CN)_6^{3-}$ and *p*-nitrophenol in five different cycles using the same film catalyst.

constant value is found to be 3.2×10^{-2} min^{-1}. It may be noted here that the rate constant values obtained for these two reactions under the present experimental conditions are dependent on the amount of the film catalysts used, and the rate of the reactions can be increased further if the amount of catalyst and/or Pt-loading are increased.

Interestingly, we observed that the catalytic property of the above Pt-loaded film is not deteriorated significantly on repeated use. After the catalytic reaction, this film catalyst is reusable after washing with distilled water for about 10 min followed by drying at 60 °C for 30 min. We have repeated the above reactions 5 times using the same film catalyst (after washing with water as mentioned above) under similar reaction conditions, and the rate constant (*k*) values of the respective reactions with respect to the different cycles are shown in Figure 12. It can be seen from Figure 12 that the film catalyst remains fairly active up to 5 cycles of reactions in both cases. The advantage of using such a catalyst is therefore many fold: (i) the catalyst can be kept inside the reaction mixture and easily separated after completion of the reaction; (ii) the spectra of the solution during the course of catalytic reaction can be monitored without any overlapping absorption originating from the catalyst. As an example, if bare Pt NPs are used for the above reaction, the absorption of Pt NPs in the UV−visible region (13, 21, 22) should affect the entire region of spectrum. For this reason, most probably, the previous reports showed the spectra in the visible region only (13, 17); (iii) the present Pt-loaded catalysts can be reused after washing with water. All previous reports in this line suffered from these problems, which we pointed out as advantages in the case of our developed catalyst. Particularly, separation of expensive catalytic nanoparticles from the reaction mixture and regeneration of their

catalytic properties are very difficult and becoming big issues and a very expensive proposition to the industry.

4. CONCLUSIONS

A unique nanocrystalline mesoporous γ-Al_2O_3 film of high thickness has been developed on glass substrates, keeping in view utilization as a catalysis support. The mesoporous films were prepared from boehmite sols using CTAB as a structure directing agent by a single dipping technique. The thickness of the heat-treated films can be adjusted up to 3 μm. The films possess worm-hole-like disordered mesophase of nanocrystalline γ-Al_2O_3 with well-accessible pores of average diameter 4.3 nm. This mesoporous γ-Al_2O_3 film can be used to host catalytically active materials to use them as reusable catalyst applicable for chemical reactions. The representative Pt-loaded film catalyst showed excellent catalytic properties in both inorganic and organic reduction systems, and has all that advantages (e.g., easy to separate, regenerate by simple washing and reuse) that people are looking for. Highly dispersed Pt NPs are found to be present inside the mesopores of the nanocrystalline γ-Al_2O_3 film matrix. This excellent mesoporous alumina film support can be used to load several other nanoparticles such as Au, Pd, Ru, Re, and bimetallic (e.g., Au—Pt, Au—Pd, etc.) nanoparticles in different concentrations useful for several other catalytic reactions. Some of the results will be reported in subsequent reports. So the development of such nanocatalysts would open up a new avenue in the area of catalysis.

Acknowledgment. Financial support from the Department of Science and Technology (DST), Government of India, under the National Nano Mission programme is gratefully acknowledged. The authors thank the Director of CG&CRI for encouragement. A.D. thanks CSIR for awarding a Junior Research Fellowship.

REFERENCES AND NOTES

(1) Sun, J.; Bao, X. *Chem.—Eur. J.* **2008**, *14*, 7478–7488.
(2) Huang, W.; Kuhn, J. N.; Tsung, C. K.; Zhang, Y.; Habas, S.E.; Yang, P.; Somorjai, G. A. *Nano Lett.* **2008**, *8*, 2027–2034.
(3) Boutros, M.; Denicourt-Nowicki, A.; Roucoux, A.; Gengembre, L.; Beaunier, P.; Gedeon, A.; Launay, F. *Chem. Commun.* **2008**, 2920–2922.
(4) Lee, J.; Orilall, M. C.; Warren, S. C.; Kamperman, M.; Disalvo, F. J.; Wiesner, U. *Nat. Mater.* **2008**, *7*, 222–228.
(5) Cortial, G.; Siutkowski, M.; Goettmann, F.; Moores, A.; Floch, P. L.; Sanchez, C. *Small* **2006**, *2*, 1042–1045. Allain, E.; Besson, S.; Durand, C.; Moreau, M.; Gacoin, T.; Boilot, J. *Adv. Funct. Mater.* **2007**, *17*, 549–554. (c) Wang, X.; Yu, J. C.; Yip, H. Y.; Wu, L.; Wong, P. K.; Lai, S. Y. *Chem.—Eur. J.* **2005**, *11*, 2997–3004.
(6) Yu, J. C.; Wang, X.; Fu, X. *Chem. Mater.* **2004**, *16*, 1523–1530.
(7) (a) Deng, W.; Toepke, M. W.; Shanks, B. H. *Adv. Funct. Mater.* **2003**, *13*, 61–65. (b) Cabrera, S.; Haskouri, J. E.; Alamo, J.; Beltran, A.; Beltran, D.; Mendioroz, S.; Marcos, M. D.; Amoros, P. *Adv. Mater.* **1999**, *11*, 379–381.
(8) (a) Yuan, Q.; Yin, A.-X.; Luo, C.; Sun, L.-D.; Zhang, Y.-W.; Duan, W.-T.; Liu, H.-C.; Yan, C.-H. *J. Am. Chem. Soc.* **2008**, *130*, 3465–3672. (b) Bagshaw, S. A.; Pinnavaia, T. J. *Angew. Chem. Int. Ed. Engl* **1996**, *35*, 1102–1105.
(9) (a) Niesz, K.; Yang, P.; Somorjai, G. A. *Chem. Commun.* **2005**, 1986–1987. (b) Morris, S. M.; Fulvio, P. F.; Jaroniec, M. *J. Am. Chem. Soc.* **2008**, *130*, 15210–15216. (c) Sun, Z.-X.; Zheng, T.-T.; Bo, Q.-B.; Vaughan, D.; Warren, M. *J. Mater. Chem.* **2008**, *18*, 5941–5947.
(10) Kuemmel, M.; Grosso, D.; Boissiere, C.; Smarsly, B.; Brezesinski, T.; Albouy, P. A.; Amenitsch, H.; Sanchez, C. *Angew. Chem. Int. Ed.* **2005**, *44*, 4589–4592.
(11) Pidol, L.; Grosso, D.; Soler-Illia, G. J. A. A.; Crepaldi, E.; Sanchez, C.; Albouy, P. A.; Amenitsch, H.; Euzen, P. *J. Mater. Chem.* **2002**, *12*, 557–564.
(12) Hicks, R. W.; Pinnavaia, T. J. *Chem. Mater.* **2003**, *15*, 78–82.
(13) Li, Y.; Petroski, J.; El-Sayed, M. A. *J. Phys. Chem. B,* **2000**, *104*, 10956–10959. Ng, Y. H.; Ikeda, S.; Harada, T.; Morita, Y.; Matsumura, M. *Chem Commun.* **2008**, 3181–3183. Wildgoose, G. G.; Banks, C. E.; Compton, R. G. *Small* **2006**, *2*, 182–193. Sarkar, J.; John, V.T.; He, J.; Brooks, C.; Gandhi, D.; Nunes, A.; Ramanath, G.; Bose, A. *Chem. Mater.* **2008**, *20*, 5301–5306. Mei, Y.; Sharma, G.; Lu, Y.; Ballauff, M.; Drechsler, M.; Irrgang, T.; Kempe, R. *Langmuir* **2005**, *21*, 12229–12234.
(14) Kundu, D.; Manna, T.; De, G. *J. Sol—Gel Sci. Technol.* **2002**, *23*, 145–150.
(15) Pal, S.; De, G. *Chem. Mater.* **2005**, *17*, 6161–6166.
(16) The room-temperature-dried, H_2PtCl_6-solution-soaked film shows a very strong absorption peak at 271 nm due to $PtCl_6^{2-}$ ions in the UV—-visible spectrum. This film after leaching out the H_2PtCl_6 (using HCl solution by ultrasonic treatments as mentioned in the Experimental Section) shows complete absence of the 271 nm peak. This indicates that the soaked H_2PtCl_6 has been leached out completely.
(17) Lu, L.; Sun, G.; Zhang, H.; Wang, H.; Xi, S.; Hu, J.; Tian, Z.; Chen, R. *J. Mater. Chem.* **2004**, *14*, 1005–1009.
(18) Rashid, M. H.; Mandal, T. K. *Adv. Funct. Mater.* **2008**, *18*, 2261–2271.
(19) Dorsey, G. A., Jr. *Anal. Chem.* **1968**, *40*, 971–972. Ji, L.; Lin, J.; Tan, K.L.; Zeng, H. C. *Chem. Mater.* **2000**, *12*, 931–939. Shen, S.C.; Chen, Q.; Chow, P. S.; Tan, G. H.; Zeng, X. T.; Wang, Z.; Tan, R. B. H. *J. Phys. Chem. C* **2007**, *111*, 700–707. De, G.; Bhattacharyya, S. *J. Mater. Chem.* **2008**, *18*, 2816–2824.
(20) De, G.; Köhn, R.; Xomeritakis, G.; Brinker, C. J. *Chem. Commun.* **2007**, 1840–1842. Crepaldi, E. L.; Soler-Illa, G.J.; Grosso, D.; Cagnol, F.; Ribot, F.; Sanchez, C. *J. Am. Chem. Soc.* **2003**, *125*, 9770–9786.
(21) Pal, S.; De, G. *Phys. Chem. Chem. Phys.* **2008**, *10*, 4062–4066. Liu, Z.; Ling, X. Y.; Lee, J. Y.; Su, X.; Gan, L. M. *J. Mater. Chem.* **2003**, *13*, 3049–3052.
(22) De, G.; Rao, C. N. R. *J. Mater. Chem.* **2005**, *15*, 891–894.

AM800241X